Original Article | Neuroimaging and Head & Neck

eISSN 2005-8330
https://doi.org/10.3348/kjr.2022.0003
Korean J Radiol 2022;23(7):742-751

Korean Journal of Radiology
KJR

Clinical Implications of Focal Mineral Deposition in the Globus Pallidus on CT and Quantitative Susceptibility Mapping of MRI

Hyojin Kim[1], Jinhee Jang[1], Junghwa Kang[2], Seungun Jang[2], Yoonho Nam[2], Yangsean Choi[1], Na-young Shin[1], Kook-Jin Ahn[1], Bum-soo Kim[1]

[1]Department of Radiology, Seoul St. Mary's Hospital, College of Medicine, The Catholic University of Korea, Seoul, Korea; [2]Division of Biomedical Engineering, Hankuk University of Foreign Studies, Yongin, Korea

Objective: To assess focal mineral deposition in the globus pallidus (GP) by CT and quantitative susceptibility mapping (QSM) of MRI scans and evaluate its clinical significance, particularly cerebrovascular degeneration.

Materials and Methods: This study included 105 patients (66.1 ± 13.7 years; 40 male and 65 female) who underwent both CT and MRI with available QSM data between January 2017 and December 2019. The presence of focal mineral deposition in the GP on QSM (GP_{QSM}) and CT (GP_{CT}) was assessed visually using a three-point scale. Cerebrovascular risk factors and small vessel disease (SVD) imaging markers were also assessed. The clinical and radiological findings were compared between the different grades of GP_{QSM} and GP_{CT}. The relationship between GP grades and cerebrovascular risk factors and SVD imaging markers was assessed using univariable and multivariable linear regression analyses.

Results: GP_{CT} and GP_{QSM} were significantly associated ($p < 0.001$) but were not identical. Higher GP_{CT} and GP_{QSM} grades showed smaller gray matter ($p = 0.030$ and $p = 0.025$, respectively) and white matter ($p = 0.013$ and $p = 0.019$, respectively) volumes, as well as larger GP volumes ($p < 0.001$ for both). Among SVD markers, white matter hyperintensity was significantly associated with GP_{CT} ($p = 0.006$) and brain atrophy was significantly associated with GP_{QSM} ($p = 0.032$) in at univariable analysis. In multivariable analysis, the normalized volume of the GP was independently positively associated with GP_{CT} ($p < 0.001$) and GP_{QSM} ($p = 0.002$), while the normalized volume of the GM was independently negatively associated with GP_{CT} ($p = 0.040$) and GP_{QSM} ($p = 0.035$).

Conclusion: Focal mineral deposition in the GP on CT and QSM might be a potential imaging marker of cerebral vascular degeneration. Both were associated with increased GP volume.

Keywords: *Globus pallidus; Iron; Calcium; Computed tomography; Quantitative susceptibility mapping*

INTRODUCTION

The basal ganglia are an area of deposition of various kinds of minerals in the brain, including iron, calcium, copper, and magnesium [1,2]. In particular, the globus pallidus (GP) is a major area of metabolism and deposition of iron and calcium [2-4]. The deposition of these two abundant and important minerals is commonly encountered in the daily practice of neuroradiology [5-8]. In addition to diffuse parenchymal deposition, there have been reports of focal deposition of iron and calcium at the medial aspect of the GP [3,5,9]. Of note, the preferential depositions of iron and calcium at the medial GP are similar but not identical [3,5,6]. Previous histological studies reported focal depositions of iron and calcium at the medial aspect of the GP in and around the penetrating arterioles and perivascular spaces, as well as in the GP parenchyma [1,3,10]. Moreover, this mineralization of the GP increased with aging [9,11].

Received: January 4, 2022 **Revised:** March 2, 2022
Accepted: March 23, 2022
Corresponding author: Jinhee Jang, MD, PhD, Department of Radiology, Seoul St. Mary's Hospital, College of Medicine, The Catholic University of Korea, 222 Banpo-daero, Seocho-gu, Seoul 06591, Korea.
• E-mail: znee@catholic.ac.kr
This is an Open Access article distributed under the terms of the Creative Commons Attribution Non-Commercial License (https://creativecommons.org/licenses/by-nc/4.0) which permits unrestricted non-commercial use, distribution, and reproduction in any medium, provided the original work is properly cited.

Copyright © 2022 The Korean Society of Radiology

Korean Journal of Radiology
KJR

The histologic location of these depositions and their associations with aging [1,9] suggest an association between the focal accumulation of minerals at the medial aspect of GP and cerebral vascular degeneration, such as small vessel disease (SVD). However, few studies have explored the association between GP mineral deposition and vascular degeneration and their clinical significance. In addition, the assessment and comparison of these two minerals, such as their prevalence and discrepancies, have not been evaluated in detail.

MRI is sensitive to both iron and calcium deposition [9]. Considering the characteristic and opposing magnetic susceptibility of iron and calcium (paramagnetic iron and diamagnetic calcium), quantitative susceptibility mapping (QSM) could be an ideal approach for their assessment [4,12,13]. However, compared to the accuracy of QSM for the assessment of iron deposition, the value of QSM for calcium has been questioned, especially in the GP [3,5]. This may be associated with the dominance of iron deposition compared to calcium deposition, resulting in a negligible contribution of diamagnetic calcium to bulk susceptibility [3,5]. Instead, additional assessment using CT could be useful to detect other features of mineral disposition at the GP, including calcium deposition [7]. Fortunately, CT is not sensitive to iron deposition in the brain other than hemorrhagic lesions [5,14]; hyperdense lesions on CT are regarded as calcific deposition regardless of co-incidental iron deposition [3,5,7].

The present study assessed the incidence and severity of iron and calcium deposition in the GP by CT and QSM and evaluated their relationship with imaging markers of SVD and cerebrovascular risk factors.

MATERIALS AND METHODS

Study Population

This study was approved by the Institutional Review Board of our institution (IRB No. KC20RISI0148). The requirement for written informed consent was waived owing to the retrospective design and anonymity of the data. Between January 2017 and December 2019, 1503 patients visited our institution's emergency department and underwent brain MRI due to clinical suspicion of a transient ischemic attack or acute ischemic stroke. The exclusion criteria were: 1) patients who underwent MRIs on other machines or without gradient echo (GRE) in their study protocols (n = 1301) and 2) those without raw GRE images required for processing QSM (n = 18), 3) lack of brain CT (n = 33), 4) different multi-echo GRE (mGRE) protocols (n = 22), 5) suboptimal MRI quality due to severe motion artifacts (n = 3), 6) known hemorrhagic lesions involving the basal ganglia that might affect image analysis (n = 5), and 7) suboptimal quality after the image processing pipeline (n = 16). Finally, the analysis included 105 participants (Fig. 1).

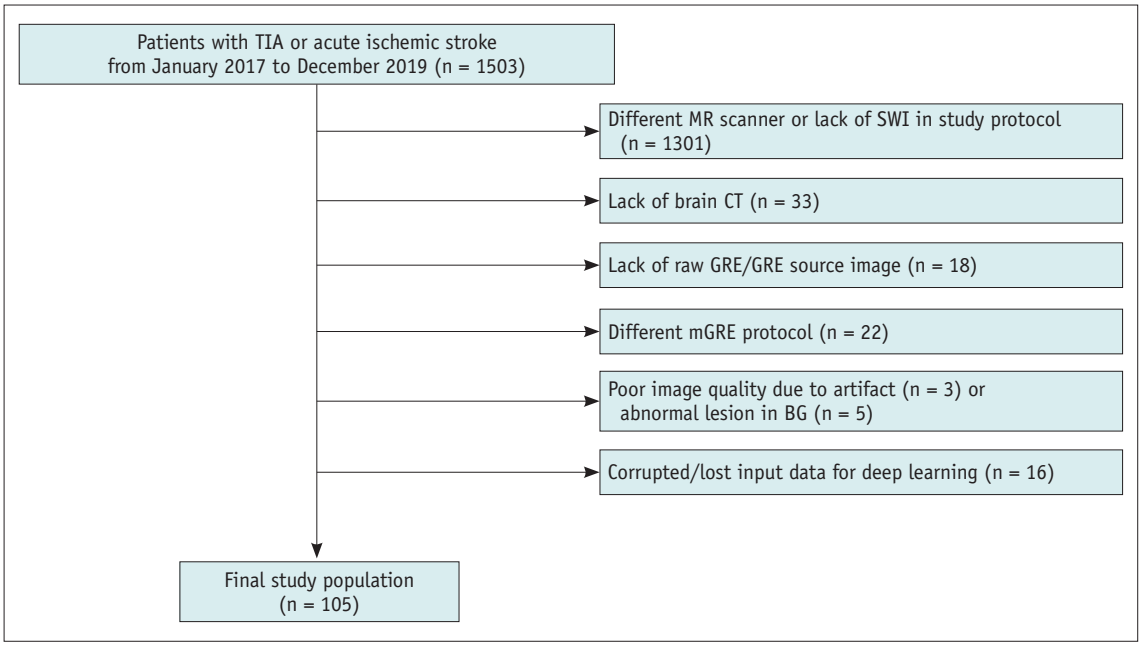

Fig. 1. Flowchart showing patient enrollment. BG = basal ganglia, GRE = gradient echo, mGRE = multi-echo GRE, SWI = susceptibility-weighted images, TIA = transient ischemic attack

https://doi.org/10.3348/kjr.2022.0003

The following cerebrovascular risk factors were assessed from the participants' medical records: hypertension, diabetes mellitus, and dyslipidemia. Hypertension was defined as systolic blood pressure ≥ 140 mm Hg, diastolic blood pressure ≥ 90 mm Hg, or treatment with antihypertensive drugs. Diabetes mellitus was defined as glycated hemoglobin (HbA1C) ≥ 6.5% or current use of anti-diabetic medications (oral hypoglycemic drugs or insulin). Dyslipidemia was defined as a total serum cholesterol level ≥ 240 mg/dL, low-density lipoprotein cholesterol level of ≥ 160 mg/dL, or current use of lipid-lowering drugs after being diagnosed with dyslipidemia.

Image Acquisition and Processing Pipeline

The overall pipeline is summarized in the Supplementary Figure 1. Brain CT scans were performed on one of two CT machines (Somatom Definition Edge or Sensation 64, Siemens Healthineers). The protocol parameters were: 100–120 kVp, 300 mAs, field of view (FOV) = 250 x 250 mm, slice thickness 4 mm, and coverage from the foramen magnum to the vertex.

The MRI images were obtained using a 3T MRI scanner (Ingenia, Philips Healthcare) with a phased-array coil with 32 channels. QSM utilizes the mGRE magnitude and phase images obtained for susceptibility-weighted imaging. The imaging parameters were: repetition time = 30 ms, echo time = 7.2/13.4/19.6/25.8 msec, fractional anisotropy = 17, FOV = 220 x 220 mm, matrix = 512 x 512, slice thickness = 2 mm. The open-source STI Suite, version 3.0 (University of California) was used for QSM [15], the details of which are described in the Supplementary Materials.

Before evaluation of the CT and MR images, each CT image was linearly co-registered to the magnitude images of GRE (i.e., containing the same spatial information as QSM) using the Linear Image Registration Tool of FMRIB Software, version 5.0 (The University of Oxford) with six degrees of

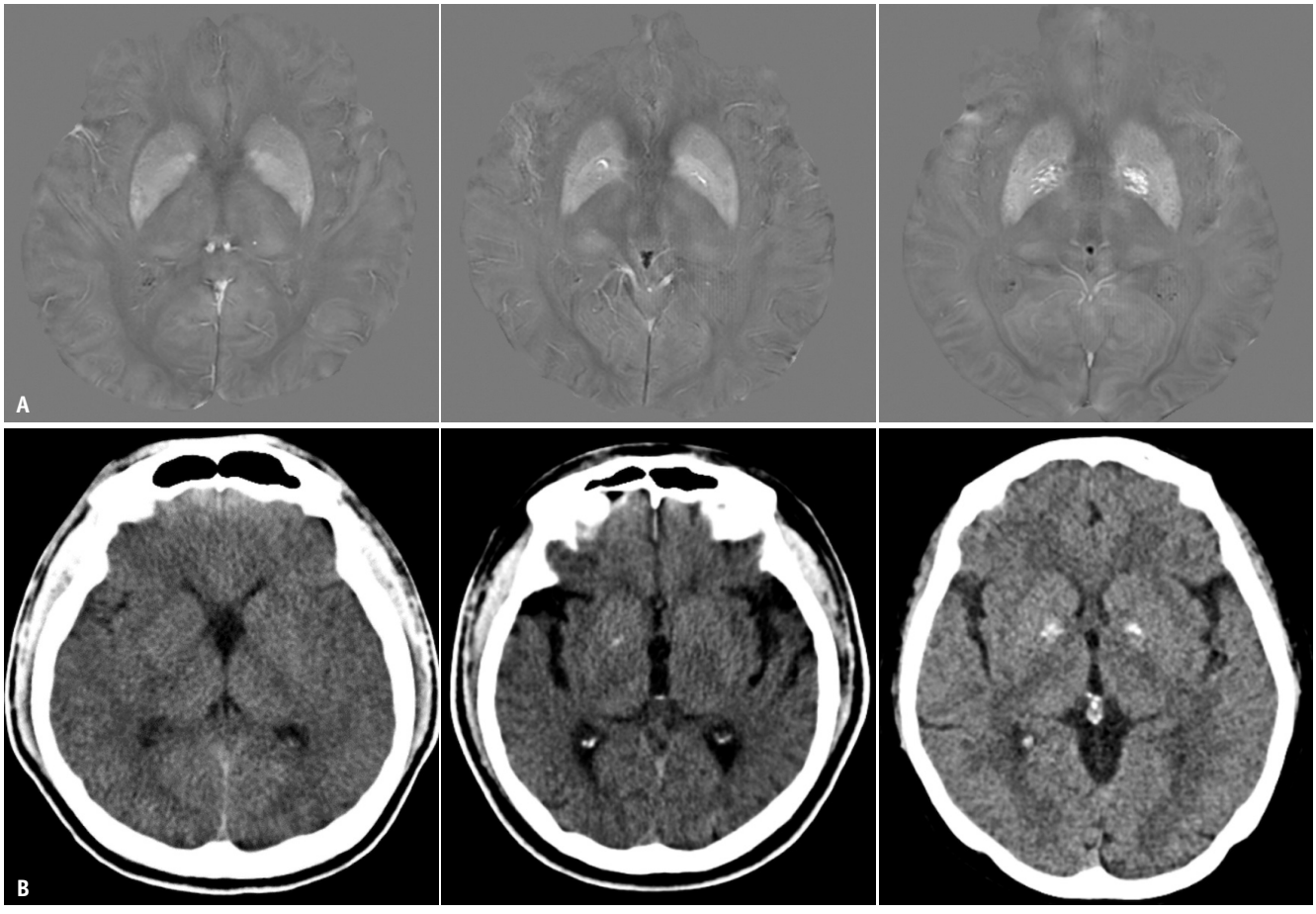

Fig. 2. Examples of the qualitative grading of focal mineral deposition in the GP.
A, B. A visual grading scale is used to assess GP_{QSM} **(A)** and GP_{CT} **(B)**. GP = globus pallidus, GP_{CT} = focal mineral deposition in the GP on CT, GP_{QSM} = focal mineral deposition in the GP on quantitative susceptibility mapping

https://doi.org/10.3348/kjr.2022.0003

Korean Journal of Radiology
KJR

freedom.

Image Assessment

Two radiologists (with 3 years and 15 years of experience with neuroimaging, respectively), who were blinded to all participants' information, reviewed the CT and MR images and graded the degree of mineral deposition in the GP and SVD findings in consensus. The presence and extent of mineral deposition in the medial aspect of the GP on QSM (GP_{QSM}) and CT (GP_{CT}) were assessed using a three-point grading scale (0, negative; 1, mild; 2, moderate to severe), which was modified from a previous grading system of mineralization in the GP (Fig. 2) [9]. For the assessment of SVD, four imaging findings were assessed as follows. White matter hyperintensities (WMH) were assessed on axial T2-weighted images using a modified Fazekas scale ranging from 0 to 3 [16]. Lacunes were defined as 3- to 15-mm cerebrospinal fluid-filled cavities located in the basal ganglia or white matter (WM) with low signal intensity on T1-weighted images and/or T2 fluid-attenuated inversion recovery and high signal intensity on T2-weighted images. Cerebral microbleeds were defined as small (usually 2–5 mm but up to 10 mm in diameter) hypointense lesions with associated blooming on T2*-weighted images or susceptibility-weighted images sequence [17]. Lacunes and cerebral microbleeds were categorized into three groups according to the number of lesions, regardless of location (1, no lesion; 2, 1–3 lesions; 3, ≥ 4 lesions). Atrophic changes in the brain were rated according to the global cortical atrophy scale (0, no atrophy; 1, mild atrophy with sulci opening; 2, moderate atrophy with gyral atrophy and volume loss; and 3, severe atrophy with knife blade appearance) [18].

We also quantitatively measured some brain structures using deep learning-based automatic segmentation of various brain structures from three-dimensional (3D) GRE data [19]. From the selected 3D volume-of-interest of the whole brain, cerebral cortex, cerebral WM, and GP, the volume of each structure was measured and normalized based on the whole brain volume of each subject. The mean CT attenuation and QSM magnetic susceptibility of the deep gray matter (GM) structures were calculated.

Statistical Analysis

We compared the clinical and radiological characteristics between GP_{QSM} and GP_{CT} grades using chi-square tests, analysis of variance (ANOVA), or Kruskal–Wallis tests. Dependencies between GP_{QSM} and GP_{CT} grades were assessed using Pearson's chi-square tests. The relationships between GP grades and imaging findings of SVD and cerebrovascular risk factors were assessed using univariable and multivariable linear regression analyses. All analyses were performed using R statistical software (version 4.0.5, R Foundation, www.R-project.org). $p < 0.05$ was considered statistically significant.

RESULTS

Incidence and Patient Distributions

This study included a total of 105 subjects (age, 66.1 years ± 13.7; 40 male and 65 female). The demographics,

Table 1. Characteristics of Study Participants (n = 105)

Parameters	Value
Age, year	66.1 ± 13.7
Sex, male:female	40:65
Interval between CT and MR, day	1.17 ± 6.74
Cerebrovascular risk factors	
Hypertension	69 (65.7)
Diabetes	38 (36.2)
Dyslipidemia	52 (49.5)
Radiologic markers of SVD	
WMH (Fazekas scale)	
0	23 (21.9)
1	39 (37.1)
2	31 (29.5)
3	12 (11.4)
Brain atrophy (GCA scale)	
0	30 (28.6)
1	40 (38.1)
2	26 (24.8)
3	9 (8.6)
Lacune (n)	
0	63 (60.0)
1–3	24 (22.9)
≥ 4	18 (17.1)
Cerebral microbleeds (n)	
0	59 (56.2)
1–3	27 (25.7)
≥ 4	19 (18.1)
Other findings	
Acute infarction	61 (58.1)
Old infarction	9 (8.7)
Old hemorrhage	5 (4.8)

Data are mean ± standard deviation or number of patients with percentage in parentheses. GCA = global cortical atrophy, SVD = small vessel disease, WMH = white matter hyperintensities

https://doi.org/10.3348/kjr.2022.0003

cerebrovascular risk factors, and radiologic findings observed on MRI, including SVD markers, are shown in Table 1. The distributions of patients according to GP_{CT} and GP_{QSM} grades are shown in Table 2. Subjects with any focal mineralization in the medial GP were older than those without focal mineralization (p = 0.032 and 0.043, respectively).

Crosstabulation of GP_{CT} and GP_{QSM} and Comparisons between GP Grades

The cross-tabulation of GP_{CT} and GP_{QSM} and comparisons between different GP grades are shown in Tables 2 and 3, respectively. Although GP_{CT} and GP_{QSM} were not identical, they showed significant dependence on each other (p < 0.001, chi-square test). About two-thirds (64/105) of the patients had the same grades of GP_{CT} and GP_{QSM} deposition in the GP. The remaining 41 subjects (39%) had a higher GP_{QSM} grade than GP_{CT} grade. Unsurprisingly, subjects with positive GP_{CT} showed higher mean attenuation than subjects with negative GP_{CT} (Fig. 3A), while subjects with positive GP_{QSM} showed higher susceptibility than subjects with negative GP_{QSM} (Fig. 3D). Subjects with positive GP_{CT} showed higher mean susceptibility in the GP than those with negative GP_{CT} (Fig. 3B). The relationship between GP_{QSM} and mean GP attenuation was not significant (Fig. 3C).

Subjects with focal mineral depositions had significantly smaller GM and WM volumes than subjects without these depositions (Table 3, Fig. 4). Meanwhile, subjects with higher grades of GP_{CT} or GP_{QSM} showed larger normalized volumes of GP (p < 0.001, both for GP_{CT} and GP_{QSM}; Table 3, Fig. 4).

Table 2. Distribution of Patients according to Grades of GP_{CT} and GP_{QSM}

GP_{QSM} \ GP_{CT}	Grade 0	Grade 1	Grade 2	Total (%)
Grade 0	37	0	0	37 (35.2)
Grade 1	25	10	0	35 (33.3)
Grade 2	9	7	17	33 (31.5)
Total (%)	71 (67.6)	17 (16.2)	17 (16.2)	

Data are number of patients with percentage out of 105 in parentheses. GP = globus pallidus, GP_{CT} = focal mineral deposition in the GP on CT, GP_{QSM} = focal mineral deposition in the GP on quantitative susceptibility mapping

Relationships between GP Grades and SVD Markers

The results of the univariable regression analysis revealed positive correlations for age and volume of GP with GP_{CT} and GP_{QSM}, while GM and WM volumes were negatively correlated with GP_{CT} and GP_{QSM} (Table 4). Among the SVD markers, WMH was significantly associated with GP_{CT} (p = 0.006). WMH showed a positive but marginal association with GP_{QSM} (p = 0.075). Brain atrophy was associated with GP_{QSM} (p = 0.032).

Multivariable regression analysis including statistically

Table 3. Comparison between Different Grades of GP_{CT} and GP_{QSM}

	GP_{CT} Grade			*P*
	0 (n = 71)	1 (n = 17)	2 (n = 17)	
Age, year	63.9 ± 8.9	74.6 ± 3.8	74.2 ± 4.6	0.032
Sex, male, %	47 (66.2)	11 (64.7)	7 (41.2)	0.157
Attenuation of GP, HU	34.0 ± 3.0	35.9 ± 3.4	36.1 ± 4.3	0.006
Susceptibility of GP, ppm	137 [122;155]	149 [133;162]	165 [151;191]	0.000
GM volume*	38.06 ± 1.41	37.14 ± 1.17	37.40 ± 1.85	0.030
WM volume*	40.04 ± 2.15	38.92 ± 1.89	38.82 ± 2.10	0.013
GP volume*	0.33 ± 0.03	0.34 ± 0.03	0.37 ± 0.04	< 0.001
	GP_{QSM} Grade			*P*
	0 (n = 37)	1 (n = 35)	2 (n = 33)	
Age, year	63.7 ± 7.7	68.9 ± 10.1	72.4 ± 6.1	0.043
Sex, male, %	21 (56.8)	26 (74.3)	18 (54.5)	0.178
Attenuation of GP, HU	34.5 ± 3.0	34.2 ± 3.0	35.1 ± 4.2	0.492
Susceptibility of GP, ppm	128 [113;146]	146 [131;157]	165 [147;190]	0.000
GM volume*	38.31 ± 1.47	37.54 ± 1.43	37.52 ± 1.48	0.025
WM volume*	40.31 ± 2.23	39.48 ± 2.06	39.12 ± 2.05	0.019
GP volume*	0.33 ± 0.024	0.33 ± 0.027	0.36 ± 0.04	< 0.001

Data are mean ± SD, number of patients, or median [interquartile range]. *Volume data are percentage relative to total intracranial volume. GM = gray matter, GP = globus pallidus, GP_{CT} = focal mineral deposition in the GP on CT, GP_{QSM} = focal mineral deposition in the GP on quantitative susceptibility mapping, HU = Hounsfield unit, WM = white matter

https://doi.org/10.3348/kjr.2022.0003

Korean Journal of Radiology
KJR

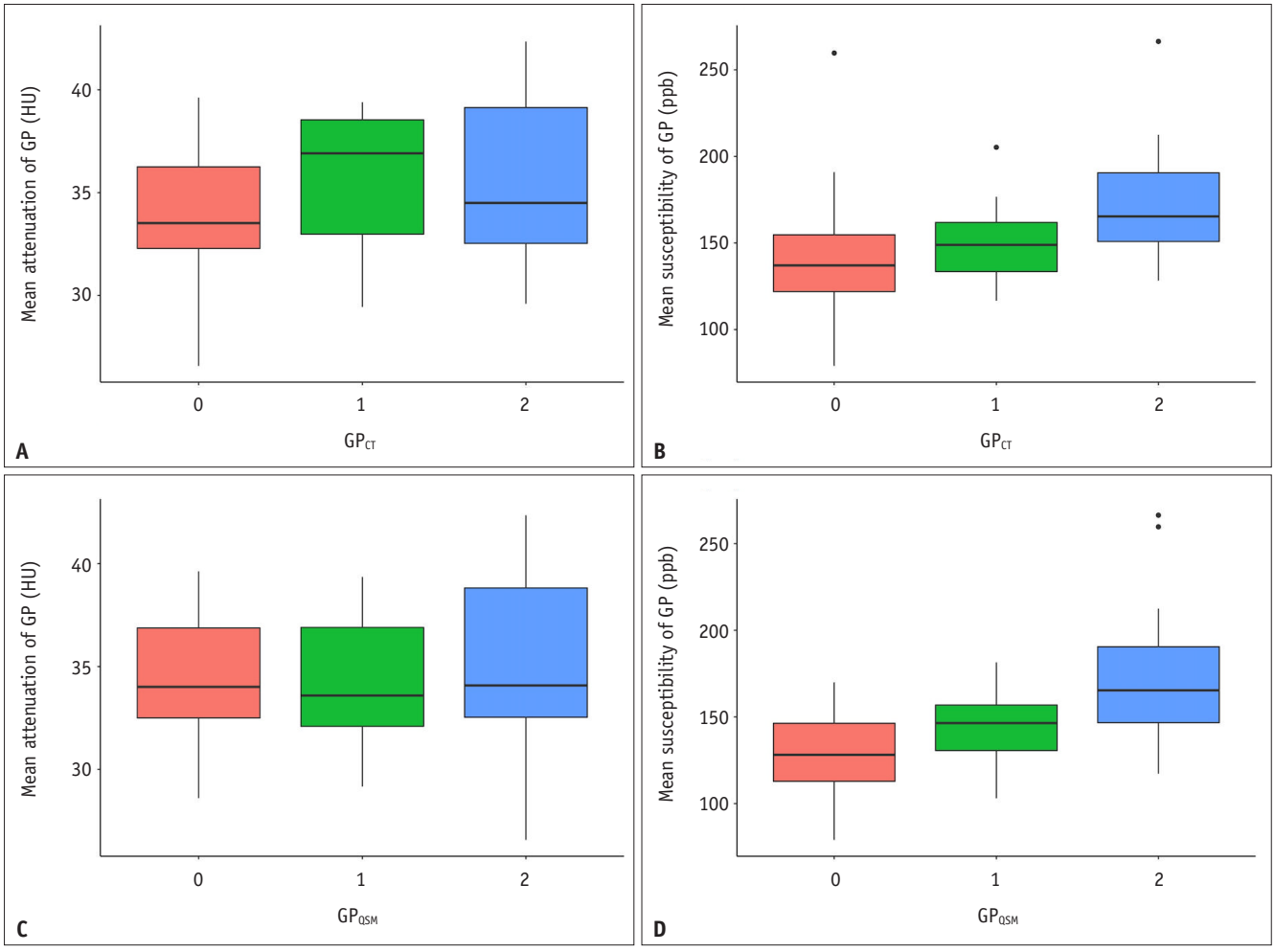

Fig. 3. Comparison of mean attenuation or susceptibility of the GP between GP_{CT} (A, B) and GP_{QSM} (C, D) grades. The mean attenuation and magnetic susceptibility differ significantly according to GP_{CT} (**A,** $p = 0.006$ and **B,** $p < 0.001$), while the mean attenuation does not differ significantly according to the GP_{QSM} (**C,** $p = 0.492$). The mean magnetic susceptibility differs significantly according to GP_{QSM} (**D,** $p < 0.001$). GP = globus pallidus, GP_{CT} = focal mineral deposition in the GP on CT, GP_{QSM} = focal mineral deposition in the GP on quantitative susceptibility mapping, HU = Hounsfield unit

significant variables in univariable analysis (Table 4) showed that the normalized volume of the GP was independently and positively associated with both GP_{CT} ($p < 0.001$) and GP_{QSM} ($p = 0.002$). The normalized GM volume was also independently negatively associated with both GP_{CT} ($p = 0.040$) and GP_{QSM} ($p = 0.035$).

DISCUSSION

This study assessed and compared focal mineral deposition at the medial aspect of the GP by CT and QSM. We investigated the incidence of these depositions as well as their associations with imaging markers of SVD. We observed a significant association between focal mineral deposition in the GP on CT and QSM. In addition, the accumulation patterns on QSM and CT were similar but not identical. We also found that mineral deposition was associated with a larger GP volume. Mineral deposition in the GP on CT was associated with WMH, while iron deposition on QSM was associated with brain atrophy.

Considering the sensitivity of QSM and CT to iron and calcium [4,7,12,13], we found a significant association between iron and calcium deposition in the medial aspect of the GP. This finding is concordant with those of previous imaging and histological studies [3,5,6]. Our systematic comparison between focal mineral deposition observed on CT and QSM showed modest correlations between the mean attenuation of GP and GP_{QSM} or GP_{CT} and good correlations between the mean magnetic susceptibility of the GP and GP_{QSM} or GP_{CT}. These findings suggest that focal deposition

https://doi.org/10.3348/kjr.2022.0003

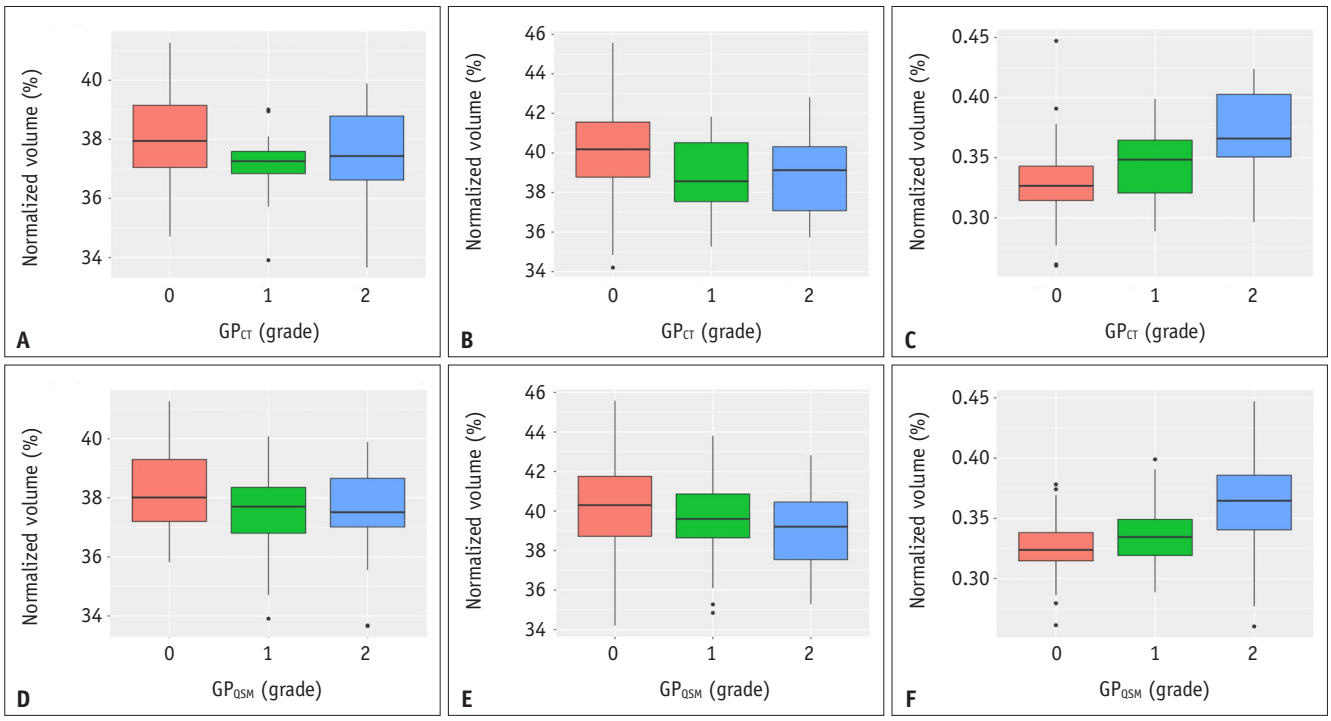

Fig. 4. Comparisons of normalized volumes of the GM, WM, and GP between GP_{CT} (A-C) and GP_{QSM} (D-F) grades. The volumes of the GM, WM, and GP differ significantly according to GP_{CT} and GP_{QSM}. The presence of mineral deposition in the GP on CT is associated with decreased GM (**A,** $p = 0.030$) and WM (**B,** $p = 0.013$) volumes. Similarly, the presence of mineral deposition in the GP on QSM is associated with decreased GM (**D,** $p = 0.025$) and WM (**E,** $p = 0.019$) volumes. Higher grades of both GP_{CT} (**C,** $p < 0.001$) and GP_{QSM} (**E,** $p < 0.001$) are associated with smaller GP volume. All p values were less than 0.05. Volume data are percentage relative to total intracranial volume. GM = gray matter, GP = globus pallidus, GP_{CT} = focal mineral deposition in the GP on CT, GP_{QSM} = focal mineral deposition in the GP on quantitative susceptibility mapping, WM = white matter

Table 4. Regression Analysis Using Generalized Linear Model for GP_{CT} and GP_{QSM}

	GP_{CT}				GP_{QSM}			
	Univariable Analysis		Multivariable Analysis		Univariable Analysis		Multivariable Analysis	
	Coefficient	*P*	Coefficient	*P*	Coefficient	*P*	Coefficient	*P*
Age	0.04	0.012	0.0004	0.986	0.036	0.022	-0.01	0.660
Sex	-0.55	0.193			0.334	0.424		
Normalized GM volume	-0.38	0.014	-0.454	0.040	-0.381	0.013	-0.41	0.035
Normalized WM volume	-0.26	0.011	-0.200	0.177	-0.233	0.025	-0.21	0.097
Normalized GP volume	25.17	0.001	31.658	< 0.001	19.180	0.007	25.58	0.002
WMH	0.65	0.006	0.136	0.696	0.407	0.075		
Brain atrophy	0.12	0.579			0.515	0.032	0.27	0.345
Lacune	0.18	0.485			0.081	0.761		
CMB	-0.07	0.778			0.207	0.444		
Hypertension	-0.44	0.305			0.058	0.892		
Diabetes	-0.05	0.895			0.070	0.868		
Dyslipidemia	-0.67	0.112			-0.280	0.494		

CMB = cerebral microbleed, GM = gray matter, GP = globus pallidus, GP_{CT} = focal mineral deposition in the GP on CT, GP_{QSM} = focal mineral deposition in the GP on quantitative susceptibility mapping, WM = white matter, WMH = white matter hyperintensities

of iron at the medial GP, represented by GP_{QSM}, could be a good surrogate for overall iron deposition in the GP [4,12]. In contrast, the mean attenuation of the GP on CT might not be a sensitive method for the quantitative measurement of mineral deposition in the GP, given the noise level in clinical CT scans.

Similar to previous studies showing age-related deposition of iron and calcium in the GP [9,11], we

https://doi.org/10.3348/kjr.2022.0003

Korean Journal of Radiology
KJR

observed a significant positive association between age and focal deposition of both iron and calcium. As previous histological studies suggested that these focal iron and calcium depositions at the medial aspect of GP occurred mainly in vascular structures [1,3,10], our results indicated that *in vivo* MRI and CT assessment of GP mineralization could be a potential imaging marker for vascular degeneration. We also observed a significant association between WMH and GP_{CT}, a marginal association between WMH and GP_{QSM}, and a significant association between aging and both GP_{CT} and GP_{QSM}. These findings suggest a potential association between SVD and vascular degeneration. Chen et al. [20] reported that intracranial arterial calcification was correlated with WMHs. Increased systemic arterial stiffness was also associated with cerebral arterial calcification [21] and larger WMH volume [22,23]. Additionally, a study using ultrasonographic parameters of penetrating arterial compliance showed that decreased pulsatility in penetrating arteries was significantly associated with WMH progression [24]. We did not observe significant associations between GP_{QSM} or GP_{CT} and cerebrovascular risk factors. Future studies with larger sample sizes are needed to clarify this finding.

Our study showed a relationship between focal calcium and iron deposition in the GP and brain volume. We observed a decreasing total GM volume but increasing GP volume with higher GP_{QSM} and GP_{CT} grades. Loss of iron and calcium homeostasis occurs with aging and in several neurodegenerative diseases [25,26]. Atrophic changes in the total GM might represent a net accumulation of tissue damage, while dense mineral deposition might be associated with neurodegeneration. We postulate that these mineral depositions may be associated with the acceleration of neuronal loss by oxidative stress, neurotoxicity, and accumulation of disease-related proteins [25,27]. Moreover, previous studies have shown that aging is associated with a decreased GP volume, but with relatively slower rates than other striatal structures [28,29]. Given the positive association between GP volume and GP_{QSM} and GP_{CT} after adjusting for aging and other potential confounders, mineral deposition might induce structural changes in the GP. Another possible explanation is that the mineralization of GP might result from different iron and calcium metabolism [30]. Increased metabolic activity of the GP might be associated with increased transport of iron and calcium to the GP via the vasculature and blood-brain barrier [31]. Further studies are required to elucidate whether mineral overload is the cause of the increased GP volume or an incidental epiphenomenon of an enlarged GP.

This study has several limitations. First, the retrospective nature of this study could be a source of unexpected bias. In addition, the cross-sectional analysis could not clarify the causes and effects. Future longitudinal studies with larger sample sizes and histopathological analyses are needed to confirm the hypothesis. Second, qualitative visual grading was used to evaluate mineralization. While this simplified grading system might be easily introduced into the clinical setting, it might not be sufficient to demonstrate its association with other clinical and radiological features. Thus, quantitative analysis may provide more statistically representative results. Third, we did not consider subject clinical backgrounds other than cerebrovascular risk factors that may have affected mineralization of the GP. Finally, single-energy CT might be limited for the differentiation of small hemorrhagic foci from calcification. However, several studies have used conventional single-energy CT as a reference tool for the detection of calcification deposition in the brain [7] and a previous study [3] showed a good correlation between calcific density on CT and vascular calcific deposition in histological studies.

In conclusion, focal iron and calcium depositions in the GP showed similar but not identical locations and patterns in CT and QSM. These depositions may be potential imaging markers of cerebral SVD. Both GP_{QSM} and GP_{CT} were significantly associated with increased GP volume, a finding that requires further evaluation to elucidate the pathophysiological mechanism and clinical significance.

Supplement

The Supplement is available with this article at https://doi.org/10.3348/kjr.2022.0003.

Availability of Data and Material

The datasets generated or analyzed during the study are available from the corresponding author on reasonable request.

Conflicts of Interest

Jinhee Jang who is on the editorial board of the *Korean Journal of Radiology* was not involved in the editorial evaluation or decision to publish this article. All remaining authors have declared no conflicts of interest.

Author Contributions

Conceptualization: Hyojin Kim, Jinhee Jang. Data curation: Hyojin Kim, Jinhee Jang. Formal analysis: Hyojin Kim, Jinhee Jang, Junghwa Kang, Seungun Jang, Yoonho Nam. Funding acquisition: Jinhee Jang. Investigation: Hyojin Kim, Jinhee Jang, Junghwa Kang, Yoonho Nam. Methodology: Hyojin Kim, Jinhee Jang. Project administration: Jinhee Jang. Resources: all authors. Software: Jinhee Jang, Junghwa Kang, Seungun Jang, Yoonho Nam. Supervision: Jinhee Jang, Yoonho Nam. Writing—original draft: Hyojin Kim, Jinhee Jang. Writing—review & editing: all authors.

ORCID iDs

Hyojin Kim
https://orcid.org/0000-0003-3098-8411
Jinhee Jang
https://orcid.org/0000-0002-3386-1208
Junghwa Kang
https://orcid.org/0000-0003-4923-8338
Seungun Jang
https://orcid.org/0000-0002-8907-8458
Yoonho Nam
https://orcid.org/0000-0003-2149-0072
Yangsean Choi
https://orcid.org/0000-0003-1674-7101
Na-young Shin
https://orcid.org/0000-0003-1157-6366
Kook-Jin Ahn
https://orcid.org/0000-0001-6081-7360
Bum-soo Kim
https://orcid.org/0000-0002-3870-6813

Funding Statement

This work was supported by National Research Foundation of Korea funded by the Korea government (MSIT) (NRF-2020R1C1C1012320) and Hankuk University of Foreign Studies Research Fund (20211238001).

REFERENCES

1. Casanova MF, Araque JM. Mineralization of the basal ganglia: implications for neuropsychiatry, pathology and neuroimaging. *Psychiatry Res* 2003;121:59-87
2. Lee S, Nam Y, Jang J, Na GH, Kim DG, Shin NY, et al. Deep gray matter iron measurement in patients with liver cirrhosis using quantitative susceptibility mapping: relationship with pallidal T1 hyperintensity. *J Magn Reson Imaging* 2018;47:1342-1349
3. Jang J, Nam Y, Jung SW, Riew TR, Kim SH, Kim IB. Paradoxical paramagnetic calcifications in the globus pallidus: an ex vivo MR investigation and histological validation study. *NMR Biomed* 2021;34:e4571
4. Bilgic B, Pfefferbaum A, Rohlfing T, Sullivan EV, Adalsteinsson E. MRI estimates of brain iron concentration in normal aging using quantitative susceptibility mapping. *Neuroimage* 2012;59:2625-2635
5. Oshima S, Fushimi Y, Okada T, Takakura K, Liu C, Yokota Y, et al. Brain mri with quantitative susceptibility mapping: relationship to ct attenuation values. *Radiology* 2020;294:600-609
6. Yamada N, Imakita S, Sakuma T, Takamiya M. Intracranial calcification on gradient-echo phase image: depiction of diamagnetic susceptibility. *Radiology* 1996;198:171-178
7. Chew AP, Gupta G, Alatakis S, Schneider-Kolsky M, Stuckey SL. Hippocampal calcification prevalence at CT: a retrospective review. *Radiology* 2012;265:504-510
8. Osborn AG, Hedlund GL, Salzman KL. *Osborn's brain e-book*. Philadelphia: Elsevier, 2017
9. Harder SL, Hopp KM, Ward H, Neglio H, Gitlin J, Kido D. Mineralization of the deep gray matter with age: a retrospective review with susceptibility-weighted MR imaging. *AJNR Am J Neuroradiol* 2008;29:176-183
10. Morris CM, Candy JM, Oakley AE, Bloxham CA, Edwardson JA. Histochemical distribution of non-haem iron in the human brain. *Acta Anat (Basel)* 1992;144:235-257
11. Aquino D, Bizzi A, Grisoli M, Garavaglia B, Bruzzone MG, Nardocci N, et al. Age-related iron deposition in the basal ganglia: quantitative analysis in healthy subjects. *Radiology* 2009;252:165-172
12. Langkammer C, Schweser F, Krebs N, Deistung A, Goessler W, Scheurer E, et al. Quantitative susceptibility mapping (QSM) as a means to measure brain iron? A post mortem validation study. *Neuroimage* 2012;62:1593-1599
13. Sun H, Walsh AJ, Lebel RM, Blevins G, Catz I, Lu JQ, et al. Validation of quantitative susceptibility mapping with Perls' iron staining for subcortical gray matter. *Neuroimage* 2015;105:486-492
14. Labranche R, Gilbert G, Cerny M, Vu KN, Soulières D, Olivié D, et al. Liver iron quantification with MR imaging: a primer for radiologists. *Radiographics* 2018;38:392-412
15. Li W, Wang N, Yu F, Han H, Cao W, Romero R, et al. A method for estimating and removing streaking artifacts in quantitative susceptibility mapping. *Neuroimage* 2015;108:111-122
16. Fazekas F, Barkhof F, Wahlund LO, Pantoni L, Erkinjuntti T, Scheltens P, et al. CT and MRI rating of white matter lesions. *Cerebrovasc Dis* 2002;13 Suppl 2:31-36
17. Wardlaw JM, Smith EE, Biessels GJ, Cordonnier C, Fazekas F, Frayne R, et al. Neuroimaging standards for research into small vessel disease and its contribution to ageing and neurodegeneration. *Lancet Neurol* 2013;12:822-838

18. Park M, Moon WJ. Structural MR imaging in the diagnosis of Alzheimer's disease and other neurodegenerative dementia: current imaging approach and future perspectives. *Korean J Radiol* 2016;17:827-845
19. Ryu K, Shin NY, Kim DH, Nam Y. Synthesizing T1 weighted MPRAGE image from multi echo GRE images via deep neural network. *Magn Reson Imaging* 2019;64:13-20
20. Chen YC, Wei XE, Lu J, Qiao RH, Shen XF, Li YH. Correlation between intracranial arterial calcification and imaging of cerebral small vessel disease. *Front Neurol* 2019;10:426
21. Park KY, Kim YB, Moon HS, Suh BC, Chung PW. Association between cerebral arterial calcification and brachial-ankle pulse wave velocity in patients with acute ischemic stroke. *Eur Neurol* 2009;61:364-370
22. Poels MM, Zaccai K, Verwoert GC, Vernooij MW, Hofman A, van der Lugt A, et al. Arterial stiffness and cerebral small vessel disease: the Rotterdam Scan Study. *Stroke* 2012;43:2637-2642
23. Zhai FF, Ye YC, Chen SY, Ding FM, Han F, Yang XL, et al. Arterial stiffness and cerebral small vessel disease. *Front Neurol* 2018;9:723
24. Lee WJ, Jung KH, Ryu YJ, Lee KJ, Kim JM, Lee ST, et al. Progression of cerebral white matter hyperintensities and the associated sonographic index. *Radiology* 2017;284:824-833
25. Mattson MP. Calcium and neurodegeneration. *Aging Cell* 2007;6:337-350
26. Li Y, Jiao Q, Xu H, Du X, Shi L, Jia F, et al. Biometal dyshomeostasis and toxic metal accumulations in the development of Alzheimer's disease. *Front Mol Neurosci* 2017;10:339
27. Ward RJ, Zucca FA, Duyn JH, Crichton RR, Zecca L. The role of iron in brain ageing and neurodegenerative disorders. *Lancet Neurol* 2014;13:1045-1060
28. Raz N, Rodrigue KM, Kennedy KM, Head D, Gunning-Dixon F, Acker JD. Differential aging of the human striatum: longitudinal evidence. *AJNR Am J Neuroradiol* 2003;24:1849-1856
29. Walhovd KB, Fjell AM, Reinvang I, Lundervold A, Dale AM, Eilertsen DE, et al. Effects of age on volumes of cortex, white matter and subcortical structures. *Neurobiol Aging* 2005;26:1261-1270
30. Rouault TA. Iron metabolism in the CNS: implications for neurodegenerative diseases. *Nat Rev Neurosci* 2013;14:551-564
31. Goswami R, Sharma R, Sreenivas V, Gupta N, Ganapathy A, Das S. Prevalence and progression of basal ganglia calcification and its pathogenic mechanism in patients with idiopathic hypoparathyroidism. *Clin Endocrinol (Oxf)* 2012;77:200-206

 https://doi.org/10.3348/kjr.2022.0003